Journal of Hydrology: Regional Studies 66 (2026) 103669

Contents lists available at ScienceDirect

Journal of Hydrology: Regional Studies

journal homepage: www.elsevier.com/locate/ejrh

Soil erosion under climate and land-use change scenarios: An integrated modelling approach for the Upper Blue Nile Basin

Legese Abebaw Getu [a,b,1,*], Sándor Szegedi [c], Hailu Kendie Addis [d], Zoltán Túri [e]

[a] Doctoral School of Earth Sciences, Landscape Protection and Environmental Geography, University of Debrecen, Egyetem tér 1, Debrecen 4032, Hungary
[b] Amhara Regional Agricultural Research Institute, Gondar Agricultural Research Center, Gondar 1337, Ethiopia
[c] Department of Meteorology, University of Debrecen, Egyetem tér 1, Debrecen 4032, Hungary
[d] Amhara Regional Agricultural Research Institute, Bahir Dar, Ethiopia
[e] Department of Physical Geography and Geoinformatics, University of Debrecen, Egyetem tér 1, Debrecen 4032, Hungary

ARTICLE INFO

Keywords:
Erosion factors
RUSLE
Erosivity
Land-use change
BMA
Ethiopian highlands

ABSTRACT

Study Region: The study was conducted in the Gumara–Maksegnit watershed of the Upper Blue Nile Basin, Ethiopia, an erosion-prone landscape that drains into Lake Tana, a hydrologically and ecologically critical freshwater system. The region is characterized by steep escarpments, highly erodible soils, and rapidly expanding agriculture, making it a hotspot of sediment generation and land degradation within the basin.

Study Focus: This study assessed past (2003), present (2023), and future (2083) soil erosion by integrating the RUSLE model with ANN-based LULC simulations, Bayesian Model Averaging of five CORDEX RCMs, and bias-corrected rainfall projections. Land-use analysis showed agricultural land expanding from 53.6% (2003) to 68.7% (2023) and projected to reach 72.1% (2083), with corresponding declines in forest and grazing areas. Rainfall erosivity increased from a range of 565–647 to 613–689 MJ mm ha^{-1} h^{-1} yr^{-1}, and is projected to rise to 756–853 (RCP4.5) and 809–907 (RCP8.5) by 2083. Mean annual soil loss increased from 30.1 t ha^{-1} yr^{-1} in 2003 to 39.2 t ha^{-1} yr^{-1} in 2023, and is projected to reach 42 t ha^{-1} yr^{-1} under land-use change alone, 43.4 and 45.9 t ha^{-1} yr^{-1} under RCP 4.5 and RCP 8.5 climate scenarios, and 46.3 and 49.2 t ha^{-1} yr^{-1} when both drivers are combined.

New Hydrological Insights for the Region: Future soil loss will increase by up to 63.5% under the combined LUC + RCP8.5 scenario, with steep northern and northeastern slopes remaining persistent erosion hotspots. Topography (LS: 39.6%) is the dominant erosion driver, while high C and P values on cultivated slopes intensify sediment generation. The results show that climate change has a stronger marginal impact than land-use change and that their interaction amplifies erosion non-linearly, underscoring the need for slope-focused, climate-adaptive soil and water conservation to protect the hydrological stability of Lake Tana.

* Corresponding author at: Doctoral School of Earth Sciences, Landscape Protection and Environmental Geography, University of Debrecen, Egyetem tér 1, Debrecen 4032, Hungary
E-mail address: legese.abebaw@science.unideb.hu (L.A. Getu).
[1] 0000-0002-7300-6249

https://doi.org/10.1016/j.ejrh.2026.103669
Received 10 December 2025; Received in revised form 10 April 2026; Accepted 22 June 2026
Available online 27 June 2026
2214-5818/© 2026 The Author(s). Published by Elsevier B.V. This is an open access article under the CC BY-NC license (http://creativecommons.org/licenses/by-nc/4.0/).

1. Introduction

Soil erosion is a primary global driver of land degradation, reducing soil fertility, agricultural productivity, and ecosystem stability (Borrelli et al., 2021; Brady and Weil, 2003; Hurni et al., 2015; Pimentel, 2006). In the Ethiopian highlands, erosion hotspots persist due to steep topography, erodible soils, intensive cultivation, and declining vegetation cover, patterns widely documented across the region (Addis and Klik, 2015; Alemayehu et al., 2020a; Nyssen et al., 2004). The Gumara–Maksegnit watershed exemplifies this vulnerability, functioning both as a hydrologically important tributary to Lake Tana and a rapidly degrading landscape exposed to accelerating climate and land-use pressures (Addis et al., 2020).

Climate change—manifested through rising temperatures, intensified rainfall, and extreme events—has increasingly altered runoff generation and sediment fluxes in the Upper Blue Nile Basin (Asfaw et al., 2021; Chakilu et al., 2022; Conway, 2011). Concurrently, land-use/land-cover (LULC) transitions such as agricultural expansion, forest loss, and grazing land decline continue to reduce vegetation cover and amplify erosion risk (Bewket and Teferi, 2009; Fenta et al., 2020; Tamene et al., 2017). Socio-economic constraints and unsustainable cultivation practices compound these pressures, further elevating hydro-erosive susceptibility (Abera et al., 2020; Adimassu et al., 2019; Belachew et al., 2020; Haregeweyn et al., 2017).

The Revised Universal Soil Loss Equation (RUSLE) is widely used for assessing long-term erosion by integrating rainfall erosivity, soil erodibility, topography, land cover, and conservation practices (Renard et al., 1997; Wischmeier and Smith, 1978). Its utility in scenario-based hydrological assessment and conservation planning has been demonstrated globally (Gayen et al., 2020; Kabir et al., 2018; Sardari et al., 2019). However, its reliability depends strongly on the quality of climate and LULC inputs. Improved rainfall projections derived from downscaled climate models and multi-model ensemble techniques enhance long-term hydro-erosive prediction, particularly when bias-corrected and weighted by performance (Eekhout and de Vente, 2019; Flint and Flint, 2012; Simmons and Splinter, 2022). Bayesian Model Averaging (BMA) provides a statistically rigorous means of weighting RCMs based on predictive skill, producing refined rainfall ensembles for erosion modeling (Massoud et al., 2020; Raftery et al., 2005).

Understanding past, present, and future LULC dynamics is equally essential for characterizing the human–environment interactions that shape erosion processes. Remote sensing enables consistent characterization of historical and current land use changes (LUC)

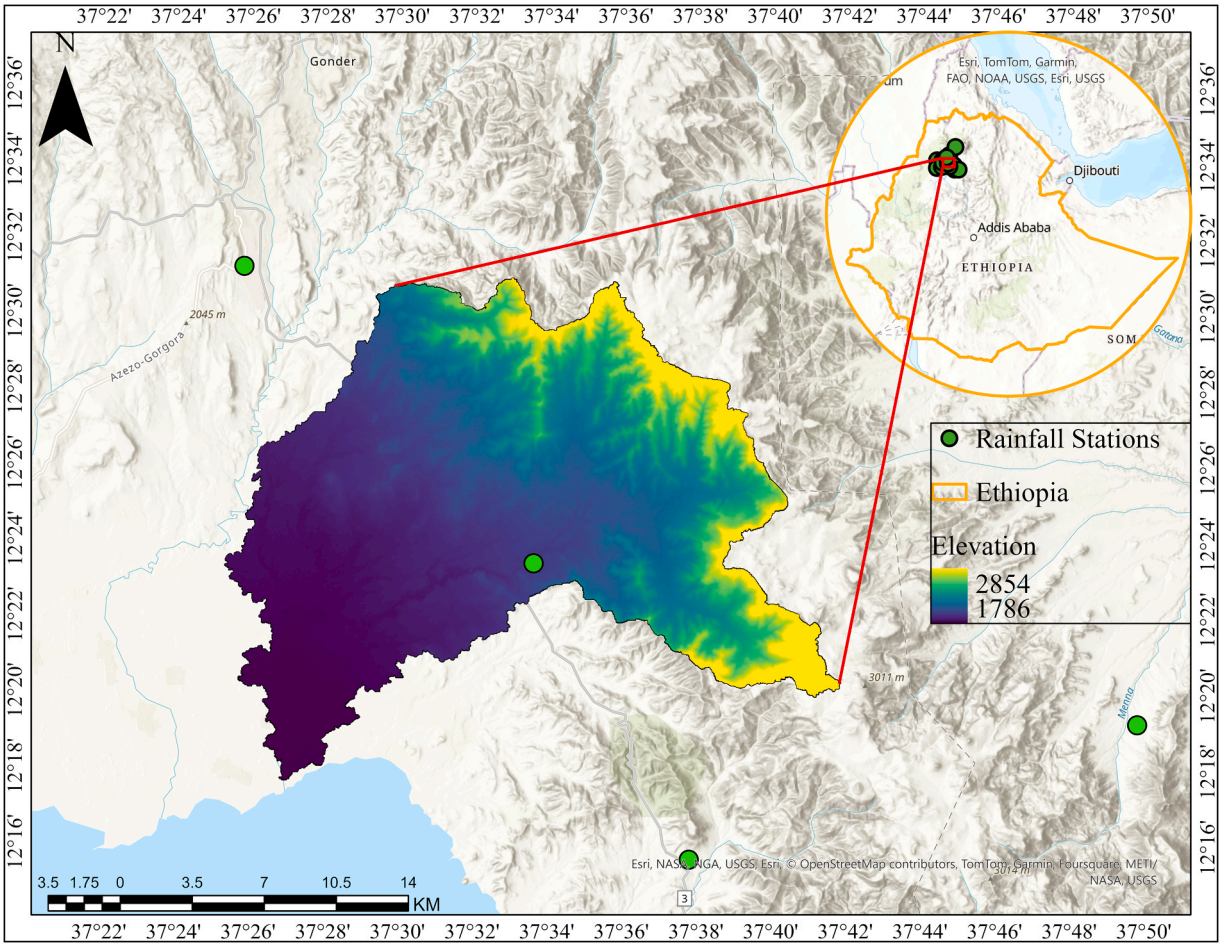


Fig. 1. Study location and distribution of rainfall stations.

(Mashala et al., 2023; Weng et al., 2023). Machine-learning-based land-use simulation tools also enable robust prediction of future landscape transitions, which is essential for assessing long-term erosion risk (Alshari and Gawali, 2022; Muhammad et al., 2022). Integrating enhanced climate projections and LULC simulations with RUSLE therefore provides a comprehensive basis for assessing future hydro-erosive responses under combined climate–LUC changes.

Despite extensive erosion research in Ethiopia, few studies have jointly examined historical, current, and future climate-LUC interactions through an integrated, multi-model framework, and none have applied such an approach to the Gumara–Maksegnit watershed. This study addresses this gap by combining RUSLE with BMA-refined climate projections and MOLUSCE-based LULC simulations to evaluate long-term erosion dynamics. Specifically, it aims to: (i) analyze spatiotemporal LULC patterns using multi-temporal satellite imagery and GIS; (ii) quantify soil erosion under historical, current, and future climate-land use scenarios; and (iii) evaluate the relative influence of RUSLE factors on erosion processes to inform targeted watershed management.

2. Methodology

2.1. Location

The Gumara–Maksegnit watershed is situated in the northwestern Ethiopian highlands within the Upper Blue Nile Basin, one of the country's most hydrologically and agriculturally significant regions. It drains south through Gondar Zuria district into Lake Tana, Ethiopia's largest freshwater lake and the primary source of the Blue Nile. The watershed covers approximately 388.7 km^2, extending from the northwestern shores of Lake Tana toward the Denkez area. Most of the watershed lies within the Gondar Zuria district, while a smaller portion extends into the adjacent Dembia district. The terrain is highly variable, with elevation ranging from 1786 to 2854 m a.s.l. (Fig. 1). This elevational range contributes to a landscape dominated by steep slopes, dissected hillsides, and narrow valley bottoms, typical of humid highland agroecological zones. The climate is monsoonal, receiving an average annual rainfall of about 1157 mm, mainly during June–September, with mean minimum and maximum temperatures of 13.3 °C and 28.5 °C, respectively (Addis et al., 2016). Productive agroclimatic conditions support high rural population densities and mixed crop, livestock systems, yet simultaneously heighten pressure on land resources. The watershed is vital for water regulation and sediment retention, affecting Lake Tana and the Blue Nile Basin. Despite its importance, the watershed is vulnerable to soil erosion due to steep terrain, heavy rainfall, agricultural expansion, and human activities that accelerate land degradation. Several studies have documented severe soil loss in the Upper Blue Nile Basin (Addis et al., 2016; Alemayehu et al., 2020a, 2020b; Nyssen et al., 2004), and the Gumara–Maksegnit watershed exhibits a similar level of vulnerability. The degradation of traditional conservation structures and the conversion of natural vegetation to farmland further exacerbate soil erosion risks to the watershed.

2.2. Datasets

Daily rainfall data for 1971–2020 were obtained from the National Meteorology Agency of Ethiopia (NMA). Among the 12 stations used, four provided continuous observations since 1971, while the remaining eight began recording in 1983. Five Regional Climate Models (RCMs) from the CORDEX-Africa database (https://esgf-metagrid.cloud.dkrz.de/) supplied historical (1971–2005) and future (2061–2090) rainfall projections under RCP 4.5 and RCP 8.5 scenarios, which represent intermediate and high-emission pathways relevant for assessing future erosivity (Patriche, 2023; Weng et al., 2023). A 30 m Shuttle Radar Topography Mission (SRTM) Digital Elevation Model (DEM) was downloaded from USGS Earth Explorer (https://earthexplorer.usgs.gov/) and used to derive topographic parameters required for the RUSLE model. Landsat imagery—Landsat 7 ETM + (2003), Landsat 8 OLI (2013), and Landsat 9 OLI (2023)—was obtained from the USGS Landsat archive and processed in Google Earth Engine (GEE) for LULC mapping. Soil texture and organic carbon data were extracted from the ISRIC SoilGrids250m database to compute the soil erodibility (K) factor. Field observations and Google Earth imagery supported the interpretation of LULC classes and enhanced understanding of local land use conditions within the watershed. The comprehensive datasets are presented in Table 1.

Table 1
Datasets.

Datasets	Resolution	Data sources	Derivation
Daily rainfall data from 12 meteorological stations (**Observed**)	Station data	NMA of Ethiopia	
MOHC-HadGEM2-CLMcom-CCLM4 (**CCLM4**) CCCma-CanESM2_CCCma-CanRCM4 (**CanRCM4**)		Coordinated Regional Climate Downscaling Experiment (CORDEX) https://esgf-metagrid.cloud.dkrz.de/	
ICHEC-EC-EARTH_KNMI-RACMO22T (**ECKNMI**) MIROC-MIROC5_SMHI-RCA4 (**MIRSMHI**) NCC-NorESM1-M_SMHI-RCA4 (**NorSMHI**)	0.44°		R Factor
Soil data	250 m	ISRIC SoilGrids250m	K Factor
Digital Elevation Model (DEM)	30 m	USGS Earth Explorer https://earthexplorer.usgs.gov/	LS & P Factor
LULC data	30 m	USGS Earth Explorer https://earthexplorer.usgs.gov/	C & P factor

2.3. Rainfall projections using BMA

The climate analysis in this study applied the Bayesian Model Averaging (BMA) framework previously developed and validated by Getu et al. (2025) to improve rainfall and erosivity estimates in the Gumara-Maksegnit watershed. Five CORDEX RCMs were first bias-corrected using CMhyd and then combined using BMA, where posterior model probabilities were assigned based on each model's historical performance against station observations. The weighted ensemble outputs were used to generate historical (1971–2000), current (2000–2020), and future (2061–2090) rainfall projections under RCP 4.5 and RCP 8.5, which were then converted into rainfall erosivity (R) using the Hurni (1985) relationship. As demonstrated by Getu et al. (2025), BMA substantially improves predictive accuracy compared to individual RCMs (R^2 = 0.69–0.85 versus 0.35–0.75; reduced bias), particularly during peak rainfall months, thereby justifying its application in this erosion-modeling framework. Full methodological details—including likelihood formulation, calibration (1971–1995), validation (1996–2005), and performance evaluation—are provided in Getu et al. (2025); therefore, only the essential steps are summarized here.

2.4. Land use change (LUC) analysis

LULC classification was performed using cloud-free Landsat imagery from three reference years: Landsat 7 ETM + (2003), Landsat 8 OLI (2013), and Landsat 9 OLI−2 (2023). Multi-month (January–April) images were used to avoid clouds and capture stable dry-season phenology. Preprocessing included cloud and shadow masking, surface reflectance calibration, and spectral harmonization to six consistent bands (Blue, Green, Red, NIR, SWIR1, SWIR2) to ensure comparability across sensors (Cao et al., 2021; Claverie et al., 2018). NDVI and NDWI were computed and added as auxiliary features to enhance class separability. The Random Forest (RF) classifier—recognized for its robustness and high accuracy in remote sensing applications (Adugna et al., 2022; Belgiu and Drăguţ, 2016)—was used for LULC classification. The RF classifier was trained using 500 trees to achieve an optimal balance between accuracy and efficiency. Training samples were derived from high-resolution imagery and manually digitized polygons representing major land cover classes: Agriculture, Forest, Grazing Land, and Settlement. The samples were split into 70% for training and 30% for validation. The classification accuracy was evaluated using confusion matrices, including overall accuracy, users' and producers' accuracies, and the Kappa coefficient.

Future LULC was modeled using the MOLUSCE plugin in QGIS. MOLUSCE applies spatial modeling approaches to simulate land-use transitions based on historical patterns (Alshari and Gawali, 2022; Muhammad et al., 2022). Transition potential was generated using 2003 and 2013 LULC maps, and an Artificial Neural Network (ANN) with a Multilayer Perceptron (MLP) architecture was used to train the model. The ANN achieved a high validation performance with a kappa value of 0.96 at a learning rate of 0.001. Validation against the reference 2023 map yielded a kappa of 0.98 and 98% correctness, demonstrating strong predictive accuracy. Building on these results, future LULC (2083) was simulated using a Cellular Automata (CA) framework. The CA model updates cell states based on transition rules and neighborhood interactions, effectively capturing spatiotemporal land-use dynamics (Jain, 2024; Muhammad et al., 2022). Using a 20-year simulation interval, four iterations were applied to generate the 2083 LULC map. Post-classification analysis, including area computation and change detection, was conducted to quantify and compare LULC changes across all study periods.

2.5. Estimate soil erosion – RUSLE model

The RUSLE is a widely applied empirical model for estimating long-term average annual soil erosion by water. It integrates environmental, land management, and terrain factors to generate spatially explicit erosion risk maps that support conservation planning (Renard et al., 1991, 1997). RUSLE is preferred in data-limited regions such as the Gumara–Maksegnit watershed because it requires fewer inputs and is simpler to implement than process-based models such as WEPP or SWAT. Annual soil loss was computed using the RUSLE equation:

$$A = R*K*L*S*C*P \quad (1)$$

Where A is annual soil loss (t ha^{-1} yr^{-1}); R is rainfall erosivity (MJ mm ha^{-1} h^{-1} yr^{-1}); K is soil erodibility (t h MJ^{-1} mm^{-1}); LS is slope length–steepness factor; C is cover-management factor; and P is conservation practice factor.

The R factor quantifies the erosive power of rainfall and strongly influences the magnitude and spatial pattern of water-induced soil loss (Renard et al., 1991; Suhara K K et al., 2023). R values for 2003, 2023, and 2083 were derived from observed and BMA-projected rainfall using Hurni (1985) empirical relationship calibrated for Ethiopian conditions:

$$R = -8.12 + 0.562 * P \quad (2)$$

Where P is the annual rainfall (mm).

The K factor represents soil susceptibility to detachment and transport as influenced by texture, structure, permeability, and organic matter (Renard et al., 1991, 1997). Clay-rich soils generally resist erosion due to greater cohesion, whereas sandy and silty soils are more prone to detachment (BASHARI et al., 2013; Xiao et al., 2022). Organic matter improves aggregate stability and reduces runoff, thus lowering K (Smith et al., 2022). K values were computed from SoilGrids data on particle size distribution and organic carbon using

the Wischmeier and Smith (1978) equation modified by Sharpley and Williams (1990):

$$K = \left\{0.2 + 0.3\ \exp\left[-0.0256SAN\left(1 - \frac{SIL}{100}\right)\right]\right\} x \left[\frac{SIL}{CLA + SIL}\right] 0.3x \left\{1 - \frac{0.25C}{[C + \exp(3.72 - 2.95C)]}\right\} x \left\{1 - \frac{0.7\left(1 - \frac{SAN}{100}\right)}{\left\{\left(1 - \frac{SAN}{100}\right) + \exp\left[-5.51 + 22.9\left(1 - \frac{SAN}{100}\right)\right]\right\}}\right\} x\ 0.1317 \quad (3)$$

Where SAN, SIL, CLA, and C are percentages of sand, silt, clay, and organic carbon, respectively. The factor 0.1317 converts the result into SI units.

The LS factor reflects the influence of topography on erosion, especially in mountainous landscapes where slope-driven runoff accelerates soil loss (Lu et al., 2020; Michalopoulou et al., 2022). LS was computed from the 30 m DEM using the Moore and Burch (1986) and Moore and Wilson (1992) formulation:

$$LS = \text{Power}\left((\text{Fac})*\frac{\text{Cell size}}{22.13}\right)^{0.4} * \text{Power}\left(\frac{(\text{Sin}(\text{Slope}*0.01745))}{0.0896}\right)^{1.3} \quad (4)$$

Where *Fac* is flow accumulation and *Slope* is slope angle (degrees). DEM preprocessing (sink filling, flow direction, and accumulation) ensured a reliable topographic representation (Panagos et al., 2015c).

The C factor accounts for the effects of vegetation cover, crop type, and surface management. Values range from 1 for bare land to as low as 0.01–0.001 for grasslands and forests (Panagos et al., 2015c; Tiruwa et al., 2021). C values for each LULC class were assigned based on established literature for the Ethiopian highlands (Haregeweyn et al., 2017; Hurni, 1985). The *P factor* reflects the impact of erosion control measures such as contouring, bunds, and terraces. Values approach 0 when conservation measures are well maintained and tend toward 1 when no practices are in place (Benavidez et al., 2018; Renard et al., 1997; Wischmeier and Smith, 1978). Field observations showed that many conservation structures in the watershed were poorly maintained, with several bunds partially filled or degraded. Thus, P values were assigned based on slope gradient and LULC following Wischmeier and Smith (1978), as applied in other Ethiopian watershed studies (Getu et al., 2022; Tiruwa et al., 2021).

Soil loss was assessed for three time periods: 2003 (historical), 2023 (current), and 2083 (future). While the period 2061–2090 represents future climate conditions, the year 2083 was selected to align with the LULC simulation framework, which applies 20-year iterative intervals from the base period. Thus, 2083 serves as a representative reference year for integrating projected climate and land-use scenarios. Seven soil loss maps produced correspond to: baseline conditions in 2003 and 2023, and five projections for 2083:

1. LUC Only: This scenario assumed changes only in LULC, which also altered the P factor since it is derived from the simulated LULC map for 2083.

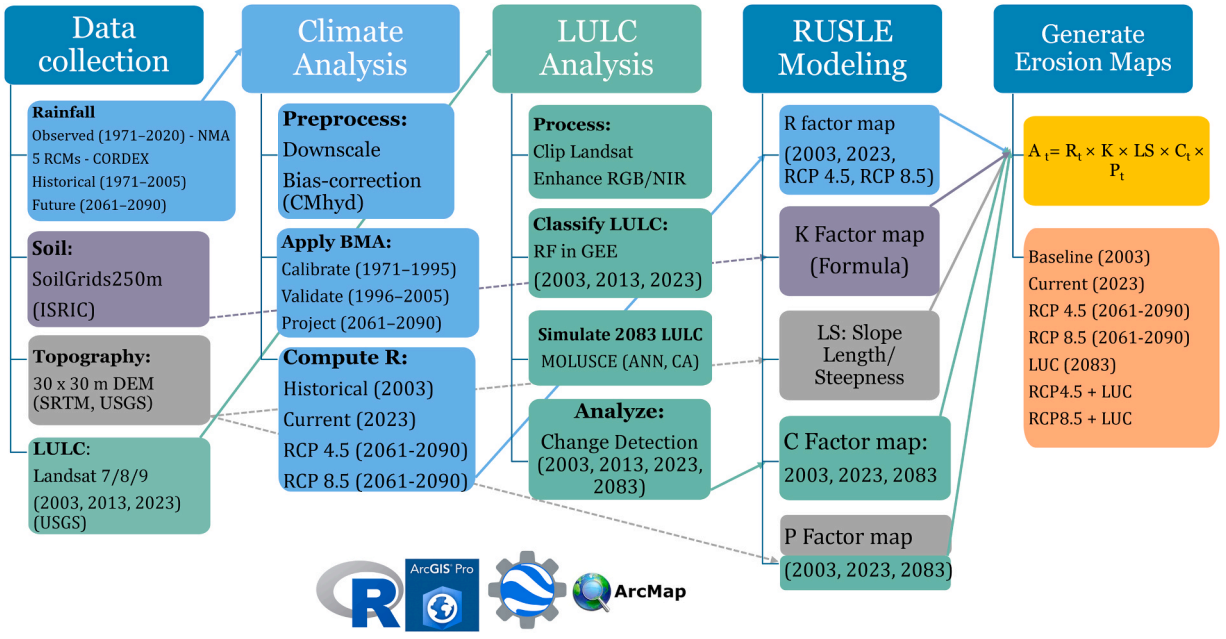


Fig. 2. Methodology framework illustrating the integrated approach for soil erosion assessment.

2. Rainfall change under RCP 4.5: This scenario evaluated the impact of rainfall changes projected under the RCP 4.5 emission scenario.
3. Rainfall change under RCP 8.5: This scenario assessed the effect of rainfall changes under the more severe RCP 8.5 climate projection.
4. Combined LUC and rainfall change under RCP 4.5: This integrated scenario analyzed the combined effects of LULC changes and rainfall projections under RCP 4.5.
5. Combined LUC and rainfall change under RCP 8.5: This scenario examined the synergistic impact of LULC changes and rainfall alterations under RCP 8.5.

Soil loss severity was classified following Morgan (2005), enabling comparison between baseline and future conditions. These scenarios allowed assessment of how climate change, land-use transitions, and their combined effects shape future soil erosion dynamics, supporting evidence-based soil and water conservation planning. The comprehensive methodological workflow is illustrated in Fig. 2.

2.6. Statistical analysis of factor influence on soil erosion

To assess the relative influence of the RUSLE factors on spatial soil erosion and analyze their combined interactions, all factor rasters (A, R, K, LS, C, P) from 2023 raster maps were resampled to a common grid and extracted into a pixel-level dataframe. Three complementary statistical methods were then used. (i) Pearson's correlation analysis was applied to identify linear relationships between soil loss and each predictor. (ii) A multiple linear regression (MLR) model with log-transformed soil loss was fitted to determine standardized coefficients, allowing comparison of each factor's effect size and direction. (iii) A Random Forest (RF) regression model with 500 trees was employed to estimate variable importance by capturing nonlinear responses and interactions that linear methods might miss. By combining correlation, MLR, and RF importance, the analysis offers a comprehensive, multi-view assessment of how each RUSLE factor influences spatial erosion patterns.

3. Results and discussions

3.1. Trends in rainfall and rainfall erosivity

Historical rainfall in the Gumara–Maksegnit watershed ranged from 1021.1 to 1165.1 mm, with a mean annual rainfall of 1092.6 mm (Fig. 3). Correspondingly, historical rainfall erosivity (R factor) varied between 565.7 and 646.9 MJ mm ha^{-1} h^{-1} yr^{-1} , averaging 605.9 MJ mm ha^{-1} h^{-1} yr^{-1} (Fig. 4). Current conditions (2001–2020) showed an upward shift in rainfall, ranging from 1107 to 1240.4 mm, which resulted in a higher R factor of 613–689.2 MJ mm ha^{-1} h^{-1} yr^{-1} . This indicates an apparent intensification of rainfall erosive power relative to the historical period. Future projections under both climate scenarios suggest a more pronounced increase. Rainfall is projected to rise to 1360.6–1531.6 mm under RCP 4.5 and 1454.7–1627.5 mm under RCP 8.5. Corresponding R factor values are expected to reach 756.6–852.6 MJ mm ha^{-1} h^{-1} yr^{-1} (RCP 4.5) and 809.4–906.5 MJ mm ha^{-1} h^{-1} yr^{-1} (RCP 8.5). These results show a consistent upward trend from the historical to current and projected periods, indicating progressively stronger rainfall erosivity across the watershed. The increase is most pronounced under the RCP 8.5 scenario, which suggests more intense and frequent erosive rainfall events. This escalation in the R factor implies greater susceptibility to soil erosion, underscoring the need for enhanced soil and water conservation strategies.

The findings show a persistent upward trend in rainfall and rainfall erosivity, consistent with ongoing regional climatic changes. Projections for RCP 4.5 and RCP 8.5 indicate further intensification, with RCP 8.5 causing the highest rainfall rates and the greatest increases in erosivity. These changes have important implications for soil erosion, as increased rainfall erosivity enhances runoff generation and sediment transport, accelerating land degradation and the loss of fertile topsoil (Panagos et al., 2015c; Renard et al.,

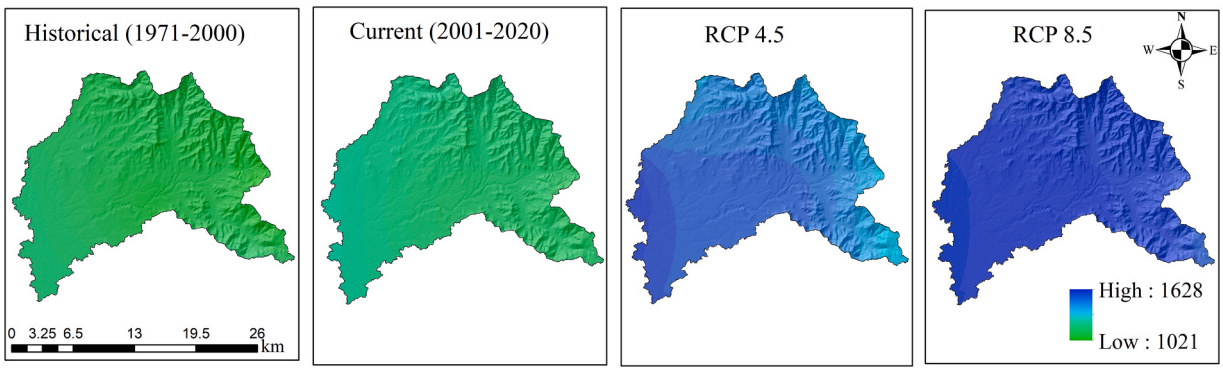


Fig. 3. Spatial distribution of mean annual rainfall across the Gumara–Maksegnit watershed for 1971–2000, 2001–2020, and 2061–2090 periods under RCP 4.5 and RCP 8.5 scenarios.

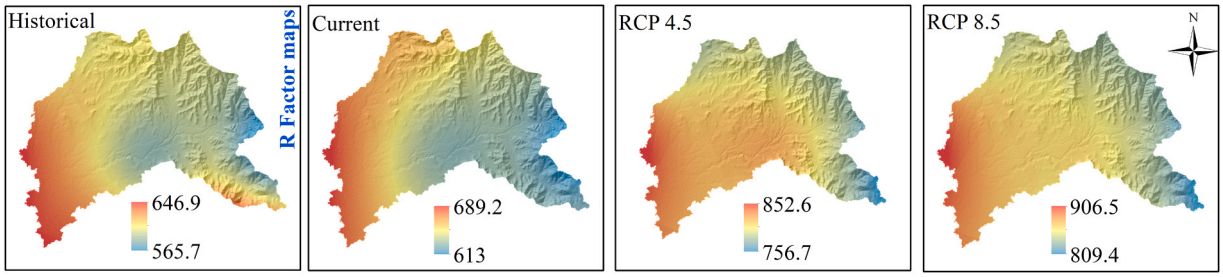


Fig. 4. R factor map for historical, current, and future (RCP 4.5 and 8.5) periods.

1997). Such impacts can reduce agricultural productivity, impair water quality, and disrupt ecosystem functions within the watershed (Borrelli et al., 2021; Hurni et al., 2015). The difference between RCP 4.5 and RCP 8.5 shows how future emission scenarios affect erosion severity. The greater impacts under RCP 8.5 highlight the risks associated with minimal climate mitigation efforts. These findings are consistent with previous studies linking intensified rainfall and climate variability to elevated erosion hazards in Ethiopia and beyond (Chakilu et al., 2022).

3.2. Soil erodibility (K)

The K factor in the Gumara–Maksegnit watershed ranged from 0.1 to 0.38 t h MJ^{-1} mm^{-1} (Fig. 5). Higher K values were concentrated in the southern and southwestern parts of the watershed, where cultivated lands dominate, while lower values occurred in the northern and northeastern areas, which are relatively more vegetated. This spatial pattern reflects the influence of land use and soil management on erodibility: continuous cultivation tends to reduce organic matter and weaken soil structure, increasing susceptibility to detachment, whereas forested areas maintain higher organic carbon and more stable aggregates (Wang et al., 2024). These results align with previous research in the Ethiopian highlands, which consistently shows that forest soils exhibit lower erodibility due to improved structure and organic matter content (Addis and Klik, 2015; Bewket and Teferi, 2009; Tamene et al., 2017). Conversely, long-term cultivation promotes loss of organic soil and aggregate breakdown, elevating K values (Fenta et al., 2020; Smith et al., 2022). The observed spatial variation highlights the importance of sustainable soil management and vegetation cover in reducing erodibility within the watershed.

3.3. LS factor

The LS factor exhibited substantial spatial variability, ranging from 0 to 742.6 with a mean of 6.8 (Fig. 5). High LS values occurred in the northern, eastern, and northeastern sub-watersheds where steep slopes and dissected terrain dominate, while low values were found in the gentler southern areas near Lake Tana. LS quantifies how slope length and steepness enhance runoff and soil transport, making it a primary driver of erosion in mountainous landscapes (Lu et al., 2020; Michalopoulou et al., 2022). Notably, zones of high LS extensively overlap with recent agricultural expansion, significantly increasing erosion sensitivity. Even small increases in R or

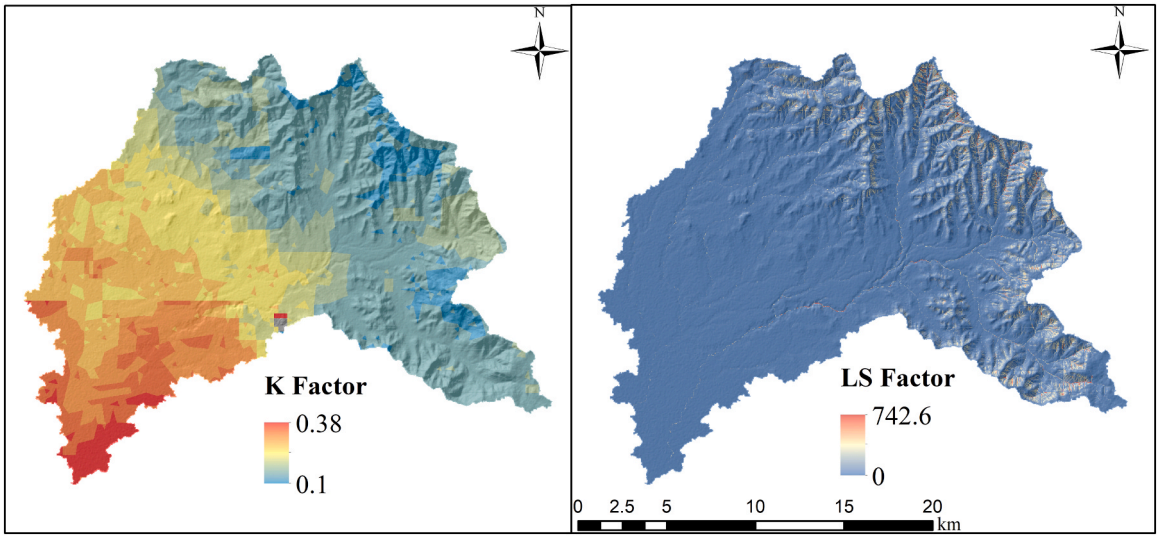


Fig. 5. K and LS factors for the Gumara-Maksegnit watershed.

reductions in C or P can trigger disproportionately high soil loss where LS is elevated (Panagos et al., 2015c; Renard et al., 1997). These high-LS areas therefore represent priority zones for slope-stabilizing conservation practices such as terraces and stone bunds (Alemayehu et al., 2020b; Haregeweyn et al., 2017).

3.4. Land use/land cover dynamics and C factor

The Gumara–Maksegnit watershed has experienced substantial LULC changes over the past two decades, with projections indicating continued transformation by 2083. As shown in Table 3, agricultural land expanded from 208.4 km^2 (53.6%) in 2003–267.1 km^2 (68.7%) in 2023 and is projected to reach 280.1 km^2 (72.1%) by 2083. Conversely, grazing land declined markedly from 130.6 km^2 (33.6%) in 2003–80.2 km^2 (20.6%) in 2023 and is expected to fall further to 69.2 km^2 (17.8%) by 2083. Forest cover also decreased from 48.8 km^2 (12.6%) in 2003–40.2 km^2 (10.3%) in 2023, with a projected reduction to 38.1 km^2 (9.8%) by 2083. Settlement areas expanded only slightly, from 0.9 km^2 in 2003–1.2 km^2 in 2023 and 1.3 km^2 in 2083. These trends indicate a continued shift toward more intensive agricultural use at the expense of grazing lands and forests. Such changes have direct implications for the C factor, as conversion from forest and grazing land to cropland generally increases vegetation disturbance, reduces protective ground cover, and elevates erosion susceptibility. The projection of LULC to 2083 assumes that historical transition dynamics remain constant over time. This represents a simplification, as future land-use patterns may be influenced by population growth, policy interventions, and socio-economic changes (Abbasnezhad et al., 2023; Zhang et al., 2022). Therefore, the simulated LULC should be interpreted as a plausible scenario rather than a deterministic prediction.

The LULC classification accuracy for 2003, 2013, and 2023 demonstrated strong and consistent performance. Producer's accuracy improved from 82% (2003) to 94.1% (2023), while user's accuracy increased from 86.6% to 92% over the same period (Table 4). Overall accuracy rose from 85% in 2003–93.4% in 2023, accompanied by an increase in the Kappa Index of Agreement from 0.78 to 0.91. These results exceed the commonly accepted minimum threshold of 85% for LULC classification reliability (Congalton, 1991), confirming that the classified maps are suitable for robust change detection and for deriving C-factor inputs for erosion modeling.

The spatial patterns of LULC transitions (Fig. 6) reveal clear and consistent trends across the watershed. Between 2003 and 2013, agricultural land increased by more than 51 km^2, mainly at the expense of grazing land and forest areas. Although the pace of expansion slowed after 2013, the same trajectory continued through 2023 and is projected to persist towards 2083. The maps show a pronounced contraction of grazing lands in the central and northern parts of the watershed, accompanied by a gradual decline in forest cover, particularly in the northeastern regions. These spatial shifts underscore the ongoing intensification of agricultural land use and the progressive encroachment into ecologically sensitive areas.

The observed LUCs align with broader regional trends in the northwestern Ethiopian highlands, where population growth and rising food demand continue to drive agricultural expansion at the expense of natural vegetation and communal grazing areas (Birhanu et al., 2024; Kindu et al., 2018; Wondie et al., 2016). The loss of forest and grazing lands reduces natural soil protection, decreases infiltration capacity, and enhances surface runoff, ultimately intensifying erosion risk (Fenta et al., 2020; Tamene et al., 2017). The projected 2083 LUC scenario suggests that, without targeted land management interventions, agricultural expansion will remain the dominant trajectory, further amplifying soil degradation, and threaten key ecosystem services.

The C factor represents the protective role of land cover against raindrop impact and surface runoff (Panagos et al., 2015c). In this study, C values were assigned to each LULC type for 2003, 2023, and 2083 based on established literature (Fig. 7). Agricultural land was assigned a relatively high C value (0.15), reflecting low surface protection due to frequent soil disturbance. Forest areas with dense and continuous vegetation had the lowest C value (0.01), indicating strong erosion control. Grazing land and settlements received intermediate values of 0.05 and 0.02, respectively. The projected expansion of agricultural land—from 53.6% in 2003–72.1% by 2083—implies an overall increase in the watershed's C factor, whereas the decline in forest cover—from 12.6% to 9.8%—reduces areas with strong protective capacity. These changes collectively point to heightened erosion susceptibility. Previous studies have reported similar patterns, noting that cultivated lands typically display higher C values due to disturbance, while forests maintain low C values through protective canopy and ground cover (Ebabu et al., 2022; Panagos et al., 2015c).

3.5. The P factor

The support practice factor (P) reflects the effectiveness of soil and water conservation (SWC) measures in reducing runoff velocity and mitigating soil erosion (Tian et al., 2021). In the Gumara–Maksegnit watershed, P values were assigned based on the interaction between land use and slope gradients, ranging from 0.1 to 1. Agricultural land was assigned lower P values (0.1–0.33), depending on

Table 3
LULC area and percentage distribution in the Gumara–Maksegnit watershed for 2003, 2013, 2023, and the projected 2083.

LULC	2003		2013		2023		2083	
	Area (km^2)	%	Area (km^2)	%	Area (km^2)	%	Area (km^2)	%
Agri. Land	208.4	53.6	259.6	66.8	267.1	68.7	280.1	72.1
Forest	48.8	12.6	42.3	10.9	40.2	10.3	38.1	9.8
Grazing Land	130.6	33.6	85.66	22.0	80.2	20.6	69.2	17.8
Settlement	0.9	0.2	1.14	0.3	1.2	0.3	1.3	0.3
Total	388.7	100	388.7	100	388.7	100	388.7	100

Table 4
Accuracy assessment of LULC classifications for 2003, 2013, and 2023 in the Gumara–Maksegnit watershed.

Accuracy	LULC 2003	LULC 2013	LULC 2023
Producer'	82.0	86.9	94.1
Users'	86.6	89.2	92.0
Omission error	18.0	13.1	5.90
Commission error	13.4	10.8	8.00
Overall accuracy	85.0	87.9	93.4
KIA	0.78	0.82	0.91

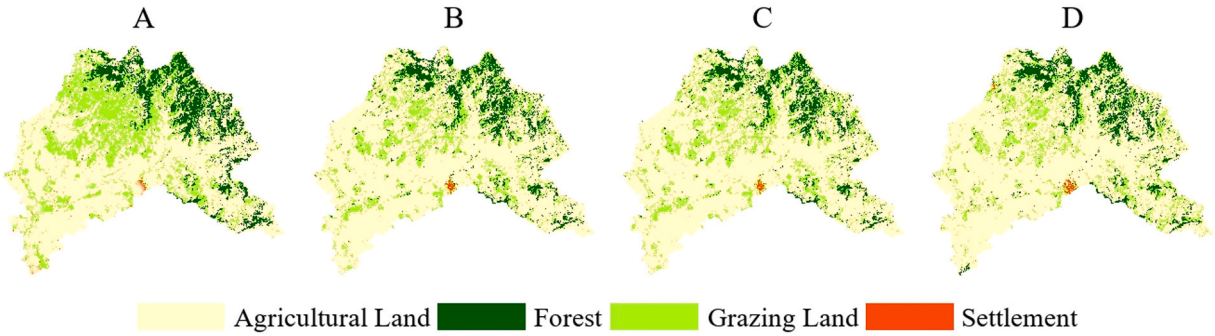


Fig. 6. LULC maps for the Gumara-Maksegnit watershed: A–D represent the years 2003, 2013, 2023, and 2083, respectively.

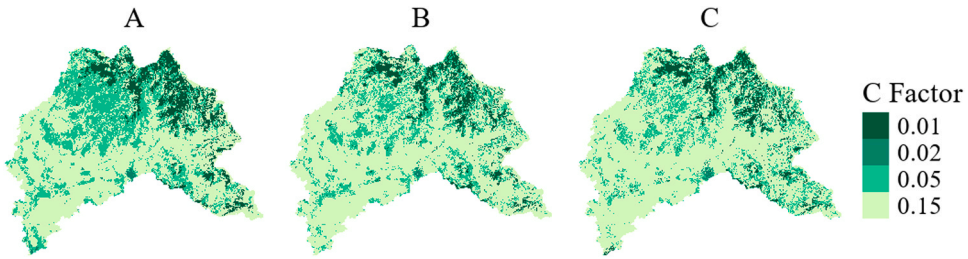


Fig. 7. The C factor maps for the Gumara-Maksegnit watershed: A–C represent 2003, 2023, and 2083, respectively.

slope, representing areas where conservation structures such as contouring or terracing can substantially reduce soil loss (Alemayehu et al., 2020a; Renard et al., 1997). Non-agricultural land, including forests and settlements, was assigned a P value of 1, indicating the absence of active conservation practices. The spatial distribution across 2003, 2023, and 2083 (Fig. 8) highlights clear temporal changes corresponding to evolving land-use patterns.

The observed increase in P values over time is closely linked to the expansion of agriculture, particularly on steeper slopes where conservation measures are either poorly implemented or absent. Similar trends reported in the Blue Nile Basin show that cropland expansion often occurs without proportional investment in SWC measures (Bewket and Teferi, 2009; Tamene et al., 2017), thereby elevating erosion risk. Field observations showed that many bunds, trenches, and terraces had degraded or filled with sediment,

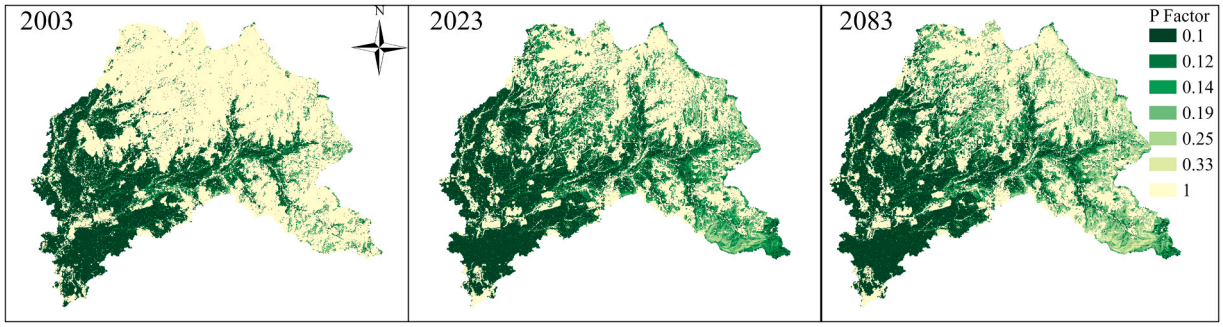


Fig. 8. P factor maps for the Gumara-Maksegnit watershed representing 2003, 2023, and 2083.

reducing their effectiveness. Similar issues in the Ethiopian highlands highlight the impact of inadequate maintenance on SWC structures' long-term protection (Getu et al., 2022; Haregeweyn et al., 2017). As emphasized by Benavidez et al. (2018), meaningful reductions in soil erosion require sustained implementation and maintenance of conservation practices to keep P values near the lower end of the scale. Although field observations indicated that many conservation structures were degraded, the adopted P values may underestimate the actual condition of poorly maintained practices, introducing uncertainty into the erosion estimates. A detailed sensitivity analysis of the P factor is beyond the scope of this study but represents an important area for future research.

3.6. Soil erosion in base periods

Modeled annual soil loss in the Gumara–Maksegnit watershed shows pronounced spatial variability driven primarily by topography, land cover, and rainfall erosivity. In 2003, soil loss ranged from near zero to over 500 t ha^{-1} yr^{-1} , with a watershed-mean value of 30.1 t ha^{-1} yr^{-1} . By 2023, the mean increased to 39.2 t ha^{-1} yr^{-1} —a 30.2% rise relative to 2003 (Fig. 9). Extreme localized erosion occurred in deeply incised valleys and steep channel slopes, where maximum values reached approximately 3400 t ha^{-1} yr^{-1} in 2003 and 5900 t ha^{-1} yr^{-1} in 2023. Areas experiencing erosion rates greater than 1000 t ha^{-1} yr^{-1} covered approximately 0.1 km^2 in 2003 and 0.3 km^2 in 2023, representing less than 0.1% of the watershed. This indicates that such extreme values are highly localized and do not influence the overall erosion assessment. Similar studies using RUSLE-based InVEST SDR model have also reported localized extreme erosion hotspots in steep and highly dissected terrains (Luo et al., 2024). Lower erosion zones were primarily located in the gentler terrain of the south and southwest, while the northern and northeastern uplands consistently displayed high erosion levels due to steep slopes combined with expanding cropland. These areas showed elevated C and P values associated with reduced vegetation cover and limited conservation practices. The spatial pattern aligns well with RUSLE principles, which predict disproportionately high soil loss in landscapes with large LS values and increasing rainfall erosivity (Panagos et al., 2015c; Renard et al., 1997).

The observed increase between 2003 and 2023 can be attributed to three primary drivers: (i) higher rainfall erosivity in the current period (Luo et al., 2024), (ii) expansion of cropland and reduction of protective vegetation (Eekhout and de Vente, 2022; Ma et al., 2025), and (iii) limited or deteriorating conservation practices on steep agricultural slopes, which raise effective P values. These findings are consistent with previous studies in the Ethiopian highlands that identify slope, land-use change, and rainfall intensity as dominant controls on erosion processes (Bewket and Teferi, 2009; Haregeweyn et al., 2017). The hotspot zones identified here, together with the documented upward trend, are supported by observed land-cover transitions and the BMA-refined increase in rainfall erosivity. Consequently, watershed management interventions should prioritize the northern and northeastern sub-watersheds and the deeply incised channel systems, where targeted soil and water conservation measures will yield the greatest benefit (Addis et al., 2020; Alemayehu et al., 2020a).

3.7. Impact of LUC and climate change on soil erosion

Scenario analysis quantified the individual and combined effects of LUC and climate change on future (2083) soil erosion. Under the LUC-only scenario, the mean soil loss reached 42 t ha^{-1} yr^{-1} , representing a 6.7% increase from 2023 and a 39.2% increase from 2003. Climate-driven changes alone produced higher erosion levels: 43.4 t ha^{-1} yr^{-1} under RCP 4.5 and 45.9 t ha^{-1} yr^{-1} ($\sigma = \pm 116$) under RCP 8.5. These results show that climate change amplifies erosion beyond the effect of LUC alone, supporting previous findings

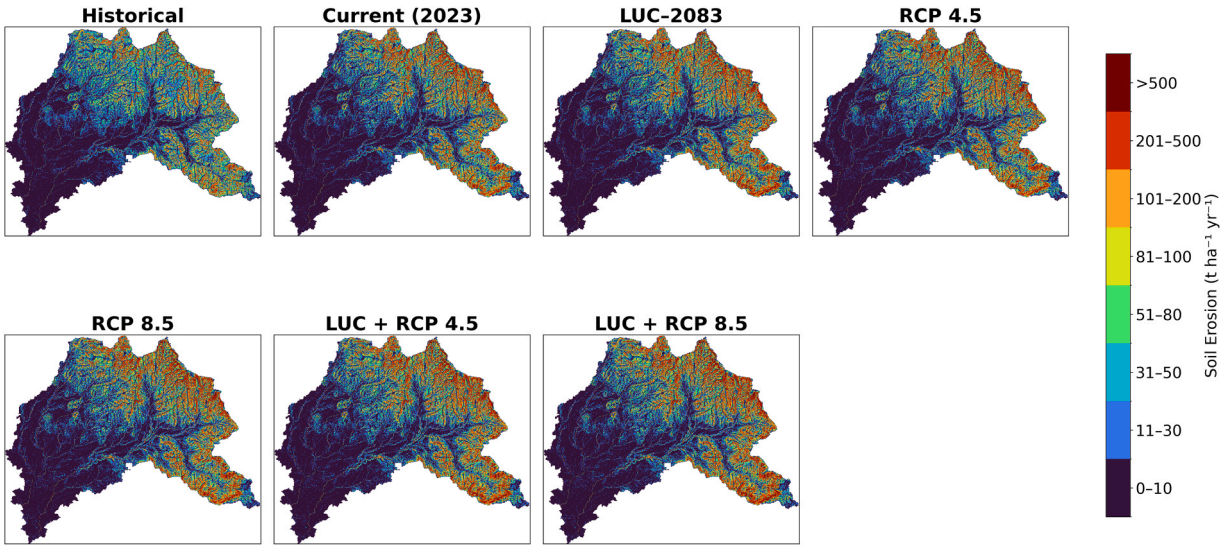


Fig. 9. Spatial and quantitative illustration of soil loss in the Gumara-Maksegnit watershed for 2003, 2023, and 2083 under LUC and climate change (RCP 4.5 and RCP 8.5) conditions.

that intensified rainfall under warming scenarios exacerbates soil loss (Ma et al., 2025; Weng et al., 2023; Xiong and Leng, 2024). When both LUC and climate projections were combined, average soil loss increased to 46.3 t ha^{-1} yr^{-1} (LUC + RCP 4.5) and 49.2 t ha^{-1} yr^{-1} (LUC + RCP 8.5). The integrated LUC + RCP 8.5 scenario represented the most severe outcome, showing a 63.5% increase relative to historical conditions. The scenario ranking (Fig. 10)—from highest to lowest mean soil loss—was: LUC + RCP 8.5 > LUC + RCP 4.5 > RCP 8.5 > RCP 4.5 > LUC-only > current > historical. The percentage-change results further emphasize that the largest increase occurs between historical conditions and the combined LUC + RCP 8.5 scenario, highlighting strong synergy between land-use intensification and climate-driven erosivity. Borrelli et al. (2020) and Fenta et al. (2020) also indicated that soil erosion risk under future climates is controlled by both anthropogenic land-cover transitions and rising rainfall intensity. Although land-use change alone results in a substantial increase in soil erosion, indicating its important role in degrading land surfaces, the marginal increase associated with climate scenarios is consistently higher. This suggests that land-use change primarily increases landscape susceptibility, while climate change—through intensified rainfall erosivity—controls the magnitude of soil loss (Dash and Maity, 2023; Luo et al., 2024; Weng et al., 2023). Therefore, both drivers are critical, but their roles are functionally different and complementary (Eekhout and de Vente, 2022; Ma et al., 2025).

3.8. Interplay between soil erosion and RUSLE factors

Pearson correlations (Fig. 11) revealed that soil loss (A) is most strongly influenced by topography (LS: 0.79), confirming the dominant role of slope in accelerating runoff and sediment detachment. Moderate positive correlations with P (0.35) and C (0.30) indicate that limited vegetation cover and ineffective conservation practices increase erosion. The negative correlations of R (–0.26) and K (–0.38) with soil loss are attributed to spatial confounding, where high rainfall and R factor values (Figs. 3 and 4) occur in relatively gentle slope areas with low LS values (Fig. 5). This spatial mismatch reduces the apparent influence of R and K and highlights the dominant role of topography. Similar observations have been made in other mountainous regions (Mahmood et al., 2024; Panagos et al., 2015a), demonstrating how strong topographic gradients can mask climatic and soil-based controls. Random Forest importance similarly highlighted LS as the leading driver (39.6%), followed by P (18.5%), C (16.7%), K (13.9%), and R (11.3%). These results align with scenario projections showing the steep northern and northeastern highlands as the most erosion-prone areas under future LUC + climate forcing (63.5% increase under RCP 8.5). This agrees with broader evidence from the Ethiopian highlands, where slope-driven hydrological acceleration consistently emerges as the primary erosion determinant (Borrelli et al., 2021; Haregeweyn et al., 2017) and highlights LS as the most influential spatial predictor (Panagos et al., 2015b). MLR standardized coefficients (P: 1.20; C: 1.06; LS: 0.68; R: –0.05; K: –0.12; $R^2 = 0.64$, $p < 0.001$) further emphasize the critical roles of conservation effectiveness and vegetation cover. High coefficients for P and C reflect deteriorating SWC structures and reduced vegetation, consistent with cropland expansion to 72.1% by 2083. This corroborates findings that poorly maintained SWC installations markedly reduce long-term erosion control (Alemayehu et al., 2020a; Haregeweyn et al., 2017).

The combined findings illustrate a key interaction: rainfall variability amplifies erosion most strongly where LULC transitions have increased C and P values on steep slopes. This synergy is particularly evident in hotspot zones, where agricultural expansion overlaps with rising R values, intensifying soil loss (Borrelli et al., 2021). Similar patterns have been reported elsewhere, showing that erosion increases disproportionately when topographic risk coincides with reduced vegetation cover or ineffective conservation (Fenta et al., 2020; Wang et al., 2024). These insights emphasize the need for integrated management strategies that simultaneously address multiple drivers—through terracing, stone bunds, and reforestation in high-LS zones; rehabilitation of degraded SWC structures to reduce P; and adoption of climate-resilient practices such as mulching, cover cropping, and agroforestry to reduce C. Such measures are essential for stabilizing soil resources and maintaining the hydrological integrity of Lake Tana inflows under future climate and land-use pressures.

Two policy-relevant inferences can be drawn from the present results. First, projected rainfall increases have a larger marginal influence on soil loss than land-use change alone, as intensified rainfall substantially elevates the R factor and drives non-linear increases in sediment detachment and transport (Eekhout and de Vente, 2019; Panagos et al., 2015a). Second, land-use change and

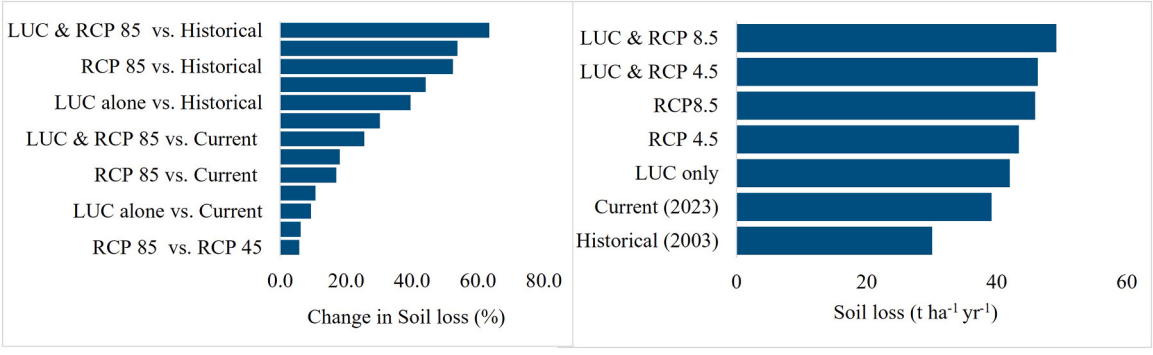


Fig. 10. Bar charts showing average annual soil loss (right) and percentage change (left) under historical, current, and future (LUC and climate change) scenarios in the Gumara–Maksegnit watershed.

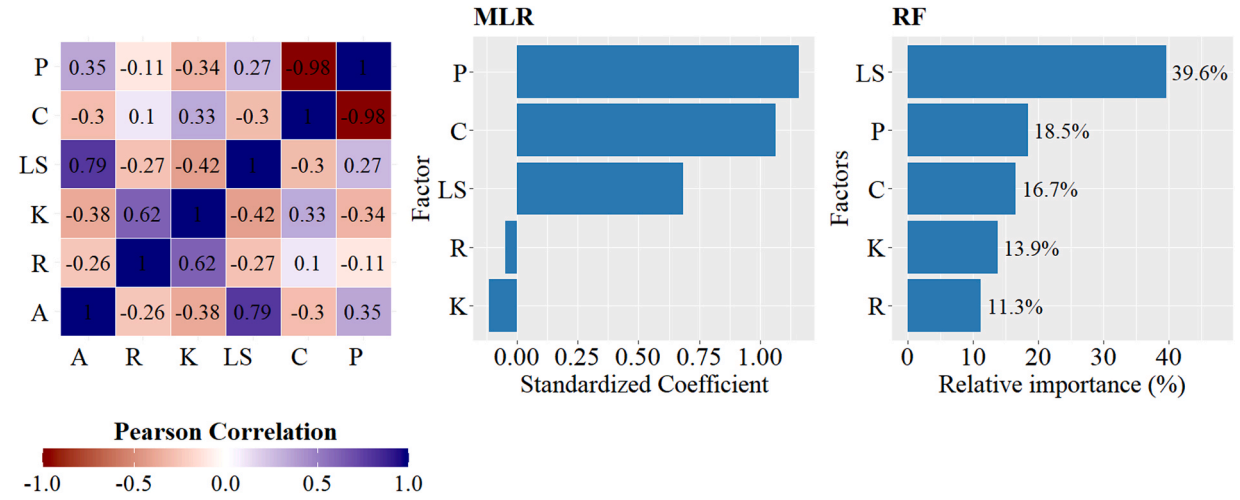


Fig. 11. Correlation and relative importance of RUSLE factors to soil erosion. Left: Pearson correlation, Middle: Relative contributions from MLR, and Right: RF feature importance.

climate change act synergistically: cropland expansion onto steep slopes heightens sensitivity to more erosive rainfall, producing greater erosion than either driver alone. This interaction aligns with broader evidence from the Ethiopian highlands (Borrelli et al., 2021; Haregeweyn et al., 2017) and underscores the need for integrated climate and land use management strategies.

3.9. Limitations/uncertainty and management implications

Downscaled and bias-corrected RCM outputs carry inherent variability that can influence the rainfall erosivity factor (R), and different correction methods may shift results (Eekhout and de Vente, 2019). Likewise, the MOLUSCE/ANN-based LULC simulation assumes the continuation of past transitions, which introduces uncertainty given potential changes in population, policy, and land management strategies. In addition, P factor is based on literature values and may not accurately represent site-specific management conditions, especially where conservation structures are degraded, which may result in underestimation of soil erosion. Thus, future work should prioritize sensitivity analysis of P factor assumptions to better quantify uncertainties arising from poorly maintained soil conservation structures. RUSLE also does not simulate gully processes, sediment routing, or deposition (Benavidez et al., 2018; Renard et al., 1997), and the absence of sediment yield data limits validation of absolute soil loss estimates. However, extreme soil loss values (>1000 t ha^{-1} yr^{-1}) are highly localized, covering less than 0.1% of the watershed, and are mainly associated with steep, gorged areas with high LS factors. Due to the multiplicative structure of RUSLE, such conditions can amplify soil loss estimates; therefore, results should be interpreted in terms of relative spatial patterns and scenario-based changes. Although the study identifies these primary sources of uncertainty, it does not quantify them numerically; doing so would require multi-model variance analysis, transition-sensitivity testing, and formal error-propagation procedures, which were beyond the scope of this work. Despite these limitations, the relative patterns, spatial hotspot distribution, and scenario-based differences remain robust, and future sensitivity analysis and validation using measured sediment yields and high-resolution hydrological monitoring would further strengthen confidence in the projections.

Management implications: Given the dominant role of LS and R on soil loss, conservation efforts should prioritize steep-slope areas, especially in the northern and northeastern sub-watersheds. Effective measures include stone bunds, bench terraces, check dams, and slope-specific land-use planning that discourages cultivation on highly erodible terrain. Maintenance of existing SWC structures is essential, as degraded or silted interventions provide limited protection (Getu et al., 2022; Haregeweyn et al., 2017). Vegetative measures—reforestation, agroforestry, grass strips, and cover crops—can lower C values and stabilize soil. In areas where rainfall erosivity is expected to rise, climate-adaptation practices such as contour farming, mulching, and vegetative buffer strips can help reduce runoff and sediment detachment (Ebabu et al., 2022; Panagos et al., 2015c; Xiong and Leng, 2024). Prioritizing interventions in modeled hotspot zones will maximize cost-effectiveness and reduce sediment delivery to Lake Tana.

4. Conclusion

This study provides the first integrated assessment of historical, current, and future soil erosion in the Gumara–Maksegnit watershed, capturing the combined effects of land-use transitions and climate-driven rainfall intensification. By integrating RUSLE with ANN-MOLUSCE-based LULC projections, BMA-refined CORDEX rainfall scenarios, and Random Forest factor diagnostics, the analysis reveals a clear long-term trajectory of increasing soil degradation over the past 20 years and into the future.

Land-use analysis shows an intense and persistent shift toward agricultural expansion—from 53.6% in 2003–68.7% in 2023—with a projected rise to 72.1% by 2083, mainly at the expense of forest and grazing land. This transition increased C and P values and

exposed steep landscapes to intensified erosion. Rainfall erosivity has also increased significantly, from a range of 565–647 MJ mm ha^{-1} h^{-1} yr^{-1} in the past to 613–689 MJ mm ha ^{1} h ^{1} yr ^{1} in the current conditions and is expected to surpass 850 (RCP 4.5) and 900 (RCP 8.5) MJ mm ha^{-1} h^{-1} yr^{-1} by 2083. Correspondingly, average soil loss rose from 30.1 t ha^{-1} yr^{-1} in 2003–39.2 t ha ^{1} yr ^{1} in 2023. Future projections indicate mean soil loss of 42 t ha^{-1} yr^{-1} under LUC alone, 43.4 and 45.9 t ha^{-1} yr^{-1} under RCP 4.5 and RCP 8.5, and 46.3 and 49.2 t ha^{-1} yr^{-1} under combined LUC + RCP 4.5 and LUC + RCP 8.5, respectively. The latter represents the most severe outcome, with a 63.5% increase relative to historical conditions. Topography was identified as the primary factor driving erosion: LS accounted for 39.6% of RF importance and showed the strongest correlation with soil loss. However, land cover (C) and conservation effectiveness (P) strongly modulate susceptibility on steep slopes. These interactions explain the persistent hotspots in the northern and northeastern highlands, where cropland expansion overlaps with high LS and rising rainfall erosivity. The results also indicate that climate change will have a larger marginal impact on future erosion than LUC alone, and their combined effect creates a synergistic impact that exceeds their individual contributions.

The management implications are clear: priority must be given to slope stabilization through terracing, stone bunds, and check dams; the rehabilitation and maintenance of existing SWC structures; reforestation and agroforestry in high-LS zones; and climate-adaptive farming practices such as residue retention and contour cultivation. Implementing these measures in identified hotspots will lead to the greatest reductions in soil erosion and sediment flow to Lake Tana. Overall, the study emphasizes an urgent need for coordinated land-use planning and climate-responsive conservation to protect soil productivity and watershed resilience amid increasing environmental changes.

CRediT authorship contribution statement

Sándor Szegedi: Writing – review & editing, Validation, Supervision. **Legese Abebaw Getu:** Writing – review & editing, Writing – original draft, Visualization, Methodology, Formal analysis, Data curation, Conceptualization. **Hailu Kendie Addis:** Writing – review & editing, Validation, Supervision, Data curation. **Zoltán Túri:** Writing – review & editing, Visualization, Validation, Supervision.

Funding

L.A.G. is supported by the Hungary Helps Agency through the Scholarship Programme for Christian Young People (SCYP) for his PhD studies. The research is supported by the NKFI Advanced 152950 project.

Declaration of Competing Interest

The authors declare that they have no known competing financial interests or personal relationships that could have appeared to influence the work reported in this paper.

Data availability

Data will be made available on request.

References

Abbasnezhad, B., Abrams, J.B., Hepinstall-Cymerman, J., 2023. Incorporating social and policy drivers into land-use and land-cover projection. Sustainability 15 (19), 14270. https://doi.org/10.3390/su151914270.

Abera, W., Assen, M., Budds, J., 2020. Determinants of agricultural land management practices among smallholder farmers in the Wanka watershed, northwestern highlands of Ethiopia. Land. Use Policy 99, 104841. https://doi.org/10.1016/J.LANDUSEPOL.2020.104841.

Addis, H.K., Abera, A., Abebaw, L., 2020. Economic benefits of soil and water conservation measures at the sub-catchment scale in the northern Highlands of Ethiopia. Progress. Phys. Geogr. Earth Environ. 44 (2), 251–266. https://doi.org/10.1177/0309133319878118.

Addis, H.K., Klik, A., 2015. Predicting the spatial distribution of soil erodibility factor using USLE nomograph in an agricultural watershed, Ethiopia. Int. Soil. Water Conserv. Res. 3 (4), 282–290. https://doi.org/10.1016/j.iswcr.2015.11.002.

Addis, H.K., Strohmeier, S., Ziadat, F., Melaku, N.D., Klik, A., 2016. Modeling streamflow and sediment using SWAT in Ethiopian highlands. Int. J. Agric. Biol. Eng. 9 (5), 51–66. https://doi.org/10.3965/j.ijabe.20160905.2483.

Adimassu, Z., Alemu, G., Tamene, L., 2019. Effects of tillage and crop residue management on runoff, soil loss and crop yield in the Humid Highlands of Ethiopia. Agric. Syst. 168, 11–18. https://doi.org/10.1016/j.agsy.2018.10.007.

Adugna, T., Xu, W., Fan, J., 2022. Comparison of random forest and support vector machine classifiers for regional land cover mapping using coarse resolution FY-3C images. Remote. Sens. 14 (3), 574. https://doi.org/10.3390/rs14030574.

Alemayehu, A.A., Getu, L.A., Addis, H.K., 2020a. Impacts of stone bunds on selected soil properties and crop yield in Gumara-Maksegnit watershed Northern Ethiopia. Cogent Food & Agric. 6 (1), 1785777. https://doi.org/10.1080/23311932.2020.1785777.

Alemayehu, A.A., Muluneh, A., Moges, A., Kendie, H., 2020b. Estimation of sediment yield and effectiveness of level stone bunds to reduce sediment loss in the Gumara-Maksegnit watershed, Nile Basin, Ethiopia. J. Soils Sediment. 20 (10), 3756–3768. https://doi.org/10.1007/s11368-020-02715-y.

Alshari, E.A., Gawali, B.W., 2022. Modeling land use change in Sana'a city of Yemen with MOLUSCE. J. Sens. 2022, 1–15. https://doi.org/10.1155/2022/7419031.

Asfaw, A., Bantider, A., Simane, B., Hassen, A., 2021. Smallholder farmers' livelihood vulnerability to climate change-induced hazards: agroecology-based comparative analysis in Northcentral Ethiopia (Woleka Sub-basin). Heliyon 7 (4), e06761. https://doi.org/10.1016/j.heliyon.2021.e06761.

BASHARI, M., MORADI, H.R., KHEIRKHAH, M.M., JAFARI-KHALEDI, M., 2013. Temporal variations of runoff and sediment in different soil clay contents using simulated conditions. Soil. Water Res. 8 (3), 124–132. https://doi.org/10.17221/60/2012-SWR.

Belachew, A., Mekuria, W., Nachimuthu, K., 2020. Factors influencing adoption of soil and water conservation practices in the northwest Ethiopian highlands. Int. Soil. Water Conserv. Res. 8 (1), 80–89. https://doi.org/10.1016/j.iswcr.2020.01.005.

Belgiu, M., Drăguţ, L., 2016. Random forest in remote sensing: a review of applications and future directions. ISPRS J. Photogramm. Remote. Sens. 114, 24–31. https://doi.org/10.1016/j.isprsjprs.2016.01.011.

Benavidez, R., Jackson, B., Maxwell, D., Norton, K., 2018. A review of the (Revised) Universal Soil Loss Equation (R/USLE): with a view to increasing its global applicability and improving soil loss estimates. https://doi.org/10.5194/hess-2018-68.
Bewket, W., Teferi, E., 2009. Assessment of soil erosion hazard and prioritization for treatment at the watershed level: case study in the Chemoga watershed, Blue Nile basin, Ethiopia. Land. Degrad. & Dev. 20 (6), 609–622. https://doi.org/10.1002/ldr.944.
Birhanu, L., Mekonen, Y., Tilahun, A., Amsalu, N., Balzter, H., 2024. Impact of land use and land cover change on soil erosion in dondor watershed, Blue Nile Basin, Northwestern Ethiopia. Sustain. (Switz.) 16 (23), 10421. https://doi.org/10.3390/su162310421.
Borrelli, P., Alewell, C., Alvarez, P., Anache, J.A.A., Baartman, J., Ballabio, C., Bezak, N., Biddoccu, M., Cerdà, A., Chalise, D., Chen, S., Chen, W., De Girolamo, A.M., Gessesse, G.D., Deumlich, D., Diodato, N., Efthimiou, N., Erpul, G., Fiener, P., Panagos, P., 2021. Soil erosion modelling: a global review and statistical analysis. Sci. Total. Environ. 780. https://doi.org/10.1016/j.scitotenv.2021.146494.
Borrelli, P., Robinson, D.A., Panagos, P., Lugato, E., Yang, J.E., Alewell, C., Wuepper, D., Montanarella, L., Ballabio, C., 2020. Land use and climate change impacts on global soil erosion by water (2015-2070). Proc. Natl. Acad. Sci. USA 117 (36), 21994–22001. https://doi.org/10.1073/pnas.2001403117.
Brady, N.C., Weil, R.R., 2003. The nature and properties of soils (15th ed., Issue 1). https://doi.org/10.16309/j.cnki.issn.1007-1776.2003.03.004.
Cao, R., Feng, Y., Chen, J., Zhou, J., 2021. A supplementary module to improve accuracy of the quality assessment band in landsat cloud images. Remote. Sens. 13 (23), 4947. https://doi.org/10.3390/rs13234947.
Chakilu, G.G., Sándor, S., Zoltán, T., Phinzi, K., 2022. Climate change and the response of streamflow of watersheds under the high emission scenario in Lake Tana sub-basin, upper Blue Nile basin, Ethiopia. J. Hydrol. Reg. Stud. 42, 101175. https://doi.org/10.1016/j.ejrh.2022.101175.
Claverie, M., Ju, J., Masek, J.G., Dungan, J.L., Vermote, E.F., Roger, J.-C., Skakun, S.V., Justice, C., 2018. The harmonized landsat and sentinel-2 surface reflectance data set. Remote. Sens. Environ. 219, 145–161. https://doi.org/10.1016/j.rse.2018.09.002.
Congalton, R.G., 1991. A review of assessing the accuracy of classifications of remotely sensed data. Remote. Sens. Environ. 37 (1), 35–46. https://doi.org/10.1016/0034-4257(91)90048-B.
Conway, D., 2011. Adapting climate research for development in Africa. WIREs Clim. Change 2 (3), 428–450. https://doi.org/10.1002/wcc.115.
Dash, S.S., Maity, R., 2023. Effect of climate change on soil erosion indicates a dominance of rainfall over LULC changes. J. Hydrol. Reg. Stud. 47, 101373. https://doi.org/10.1016/j.ejrh.2023.101373.
Ebabu, K., Tsunekawa, A., Haregeweyn, N., Tsubo, M., Adgo, E., Fenta, A.A., Meshesha, D.T., Berihun, M.L., Sultan, D., Vanmaercke, M., Panagos, P., Borrelli, P., Langendoen, E.J., Poesen, J., 2022. Global analysis of cover management and support practice factors that control soil erosion and conservation. Int. Soil. Water Conserv. Res. 10 (2), 161–176. https://doi.org/10.1016/j.iswcr.2021.12.002.
Eekhout, J.P.C., de Vente, J., 2019. The implications of bias correction methods and climate model ensembles on soil erosion projections under climate change. Earth Surf. Process. Landf. 44 (5), 1137–1147. https://doi.org/10.1002/esp.4563.
Eekhout, J.P.C., de Vente, J., 2022. Global impact of climate change on soil erosion and potential for adaptation through soil conservation. Earth-Sci. Rev. 226, 103921. https://doi.org/10.1016/j.earscirev.2022.103921.
Fenta, A.A., Tsunekawa, A., Haregeweyn, N., Poesen, J., Tsubo, M., Borrelli, P., Panagos, P., Vanmaercke, M., Broeckx, J., Yasuda, H., Kawai, T., Kurosaki, Y., 2020. Land susceptibility to water and wind erosion risks in the East Africa region. Sci. Total. Environ. 703, 135016. https://doi.org/10.1016/j.scitotenv.2019.135016.
Flint, L.E., Flint, A.L., 2012. Downscaling future climate scenarios to fine scales for hydrologic and ecological modeling and analysis. Ecol. Process. 1 (1), 2. https://doi.org/10.1186/2192-1709-1-2.
Gayen, A., Saha, S., Pourghasemi, H.R., 2020. Soil erosion assessment using RUSLE model and its validation by FR probability model. Geocarto Int. 35 (15), 1750–1768. https://doi.org/10.1080/10106049.2019.1581272.
Getu, L.A., Nagy, A., Addis, H.K., 2022. Soil loss estimation and severity mapping using the RUSLE model and GIS in Megech watershed, Ethiopia. Environ. Chall. 8, 100560. https://doi.org/10.1016/J.ENVC.2022.100560.
Getu, L.A., Sándor, S., Zoltán, T., Addis, H.K., 2025. Bayesian model averaging approach to predict future rainfall erosivity in the Gumara-Maksegnit watershed, Ethiopia. Environ. Sustain. Indic. 28, 101012. https://doi.org/10.1016/j.indic.2025.101012.
Haregeweyn, N., Tsunekawa, A., Poesen, J., Tsubo, M., Meshesha, D.T., Fenta, A.A., Nyssen, J., Adgo, E., 2017. Comprehensive assessment of soil erosion risk for better land use planning in river basins: case study of the Upper Blue Nile River. Sci. Total. Environ. 574, 95–108. https://doi.org/10.1016/j.scitotenv.2016.09.019.
Hurni, H.1985. Conservation Systems in Ethiopia. *Pla Sentis, 1.* (Edt.), 674, 1–20.
Hurni, K., Zeleke, G., Kassie, M., Tegegne, B., Kassawmar, T., Teferi, E., Moges, A., Tadesse, D., Ahmed, M., Degu, Y., Kebebew, Z., Hodel, E., Amdihun, A., Mekuriaw, A., Debele, B., Deichert, G., Hurni, H., 2015. The economics of land degradation. ethiopia case study. soil degradation and sustainable land management in the rainfed agricultural areas of Ethiopia: an assessment of the economic implications. Report. Econ. Land. Degrad. Initiat. 94.
Jain, M., 2024. Future land use and land cover simulations with cellular automata-based artificial neural network: a case study over Delhi megacity (India). Heliyon 10 (14), e34662. https://doi.org/10.1016/j.heliyon.2024.e34662.
Kabir, U., Mir, A.M., Sajana, M., 2018. Assessment of land cover change and its impact on changes in soil erosion risk in Nepal. Sustain. (Switz.) 10 (12). https://doi.org/10.3390/su10124715.
Kindu, M., Schneider, T., Döllerer, M., Teketay, D., Knoke, T., 2018. Scenario modelling of land use/land cover changes in Munessa-Shashemene landscape of the Ethiopian highlands. *622–623* Sci. Total. Environ. 534–546. https://doi.org/10.1016/j.scitotenv.2017.11.338.
Lu, S., Liu, B., Hu, Y., Fu, S., Cao, Q., Shi, Y., Huang, T., 2020. Soil erosion topographic factor (LS): Accuracy calculated from different data sources. CATENA 187, 104334. https://doi.org/10.1016/j.catena.2019.104334.
Luo, C., Pu, S., Yu, G., 2024. Investigating the impact of climate and land use changes on soil erosion in the Anning River basin in China. Front. Earth Sci. 12. https://doi.org/10.3389/feart.2024.1416387.
Ma, D., Peng, S., Lin, Z., 2025. Towards a more comprehensive scenario analysis: response of soil erosion to future land use and climate change in the Central Yunnan Urban Agglomeration, China. J. Environ. Manag. 376, 124523. https://doi.org/10.1016/j.jenvman.2025.124523.
Mahmood, S., Naeem, N., Ahamad, M.I., Tariq, Z., Song, J., 2024. Spatial modeling of soil erosion potential in the Panjkora Basin, Eastern Hindu Kush: integrated RUSLE and geospatial approaches. Environ. Dev. Sustain. https://doi.org/10.1007/s10668-024-05709-9.
Mashala, M.J., Dube, T., Mudereri, B.T., Ayisi, K.K., Ramudzuli, M.R., 2023. A systematic review on advancements in remote sensing for assessing and monitoring land use and land cover changes impacts on surface water resources in semi-arid tropical environments. Remote. Sens. 15 (16), 3926. https://doi.org/10.3390/rs15163926.
Massoud, E.C., Lee, H., Gibson, P.B., Loikith, P., Waliser, D.E., 2020. Bayesian model averaging of climate model projections constrained by precipitation observations over the contiguous United States. J. Hydrometeorol. 21 (10), 2401–2418. https://doi.org/10.1175/JHM-D-19-0258.1.
Michalopoulou, M., Depountis, N., Nikolakopoulos, K., Boumpoulis, V., 2022. The significance of digital elevation models in the calculation of LS factor and soil erosion. Land 11 (9), 1592. https://doi.org/10.3390/land11091592.
Moore, I.D., Burch, G.J., 1986. Physical basis of the length-slope factor in the universal soil loss equation. Soil. Sci. Soc. Am. J. 50 (5), 1294–1298. https://doi.org/10.2136/sssaj1986.03615995005000050042x.
Moore, I.D., Wilson, J.P., 1992. Length-slope factors for the revised universal soil loss equation: simplified method of estimation. J. Soil. Water Conserv. 47 (5), 423–428. https://doi.org/10.1080/00224561.1992.12456740.
Morgan, R.P.C., 2005. Soil Erosion and Conservation, 3rd ed. Blackwell Publishing company.
Muhammad, R., Zhang, W., Abbas, Z., Guo, F., Gwiazdzinski, L., 2022. Spatiotemporal change analysis and prediction of future land use and land cover changes using QGIS MOLUSCE plugin and remote sensing big data: a case study of Linyi, China. Land 11 (3), 419. https://doi.org/10.3390/land11030419.
Nyssen, J., Poesen, J., Moeyersons, J., Deckers, J., Haile, M., Lang, A., 2004. Human impact on the environment in the Ethiopian and Eritrean highlands—a state of the art. Earth-Sci. Rev. 64 (3–4), 273–320. https://doi.org/10.1016/S0012-8252(03)00078-3.

Panagos, P., Ballabio, C., Borrelli, P., Meusburger, K., Klik, A., Rousseva, S., Tadić, M.P., Michaelides, S., Hrabalíková, M., Olsen, P., Aalto, J., Lakatos, M., Rymszewicz, A., Dumitrescu, A., Beguería, S., Alewell, C., 2015a. Rainfall erosivity in Europe. Sci. Total. Environ. 511, 801–814. https://doi.org/10.1016/j.scitotenv.2015.01.008.

Panagos, P., Borrelli, P., Meusburger, K., 2015b. A new European slope length and steepness factor (LS-Factor) for modeling soil erosion by water. Geosciences 5 (2), 117–126. https://doi.org/10.3390/geosciences5020117.

Panagos, P., Borrelli, P., Poesen, J., Ballabio, C., Lugato, E., Meusburger, K., Montanarella, L., Alewell, C., 2015c. The new assessment of soil loss by water erosion in Europe. Environ. Sci. & Policy 54, 438–447. https://doi.org/10.1016/j.envsci.2015.08.012.

Patriche, C.V., 2023. Applying RUSLE for soil erosion estimation in Romania under current and future climate scenarios. Geoderma Reg. 34, e00687. https://doi.org/10.1016/j.geodrs.2023.e00687.

Pimentel, D., 2006. Soil erosion: a food and environmental threat. Environ. Dev. Sustain. 8 (1), 119–137. https://doi.org/10.1007/s10668-005-1262-8.

Raftery, A.E., Gneiting, T., Balabdaoui, F., Polakowski, M., 2005. Using Bayesian model averaging to calibrate forecast ensembles. Mon. Weather. Rev. 133 (5), 1155–1174. https://doi.org/10.1175/MWR2906.1.

Renard, K., Foster, G.R., Weesies, G.A., Porter, J.I., 1991. Revised universal soil loss equation (RUSLE). J. Soil. Water Conserv. 30–33. https://doi.org/10.1007/springerreference_77104.

Renard, K., Foster, G., Weesies, G., McCool, D., Yoder, D., 1997. Predicting soil erosion by water: a guide to conservation planning with the revised universal soil loss equation (RUSLE)..

Sardari, M.R.A., Bazrafshan, O., Panagopoulos, T., Sardooi, E.R., 2019. Modeling the impact of climate change and land-use change scenarios on soil erosion at the minab dam watershed. Sustain. (Switz.) 11 (12). https://doi.org/10.3390/su10023353.

Sharpley, A.N., Williams, J.R., 1990. EPIC — Erosion / productivity impact calculator (1768)..

Simmons, J.A., Splinter, K.D., 2022. A multi-model ensemble approach to coastal storm erosion prediction. Environ. Model. & Softw. 150, 105356. https://doi.org/10.1016/j.envsoft.2022.105356.

Smith, D.J., Snead, M., Thompson, T.M., 2022. Soil amended with organic matter increases fluvial erosion resistance of cohesive streambank soil. J. Geophys. Res. Biogeosciences 127 (6). https://doi.org/10.1029/2021JG006723.

Suhara K K, S., Varughese, A., Sunny, A.C., Krishna P R, A., 2023. Erosivity factor of the revised universal soil loss equation (RUSLE) - a systematized review. Curr. World Environ. 18 (2), 433–445. https://doi.org/10.12944/CWE.18.2.02.

Tamene, L., Adimassu, Z., Ellison, J., Yaekob, T., Woldearegay, K., Mekonnen, K., Thorne, P., Le, Q.B., 2017. Mapping soil erosion hotspots and assessing the potential impacts of land management practices in the highlands of Ethiopia. Geomorphology 292, 153–163. https://doi.org/10.1016/j.geomorph.2017.04.038.

Tian, P., Zhu, Z., Yue, Q., He, Y., Zhang, Z., Hao, F., Guo, W., Chen, L., Liu, M., 2021. Soil erosion assessment by RUSLE with improved P factor and its validation: case study on mountainous and hilly areas of Hubei Province, China. Int. Soil. Water Conserv. Res. 9 (3), 433–444. https://doi.org/10.1016/j.iswcr.2021.04.007.

Tiruwa, D.B., Khanal, B.R., Lamichhane, S., Acharya, B.S., 2021. Soil erosion estimation using geographic information system (GIS) and revised universal soil loss equation (RUSLE) in the Siwalik Hills of Nawalparasi, Nepal. J. Water Clim. Change 12 (5), 1958–1974. https://doi.org/10.2166/wcc.2021.198.

Wang, L., Guo, M., Chen, Z., Zhang, X., Zhou, P., Liu, X., Qi, J., Wan, Z., Xu, J., Zhang, S., 2024. Quantifying the contributions of factors influencing the spatial heterogeneity of soil aggregate stability and erodibility in a Mollisol watershed. CATENA 239, 107941. https://doi.org/10.1016/j.catena.2024.107941.

Weng, X., Zhang, B., Zhu, J., Wang, D., Qiu, J., 2023. Assessing land use and climate change impacts on soil erosion caused by water in China. Sustainability 15 (10), 7865. https://doi.org/10.3390/su15107865.

Wischmeier, W.H., Smith, D.D., 1978. Predicting rainfall erosion losses: a guide to conservation planning Beltsville. Md. U. S. Dep. Agric. Agric. Handb. No. *537*.

Wondie, M., Schneider, W., Katzensteiner, K., Mansberger, R., Teketay, D., 2016. Modelling the dynamics of landscape transformations and population growth in the highlands of Ethiopia using remote-sensing data. Int. J. Remote. Sens. 37 (23), 5647–5667. https://doi.org/10.1080/01431161.2016.1246773.

Xiao, H., Guo, P., Zhang, Q., Hu, H., Hong, H., Zhang, L., Yang, Y., Xia, Z., Li, M., Kang, H., Zhang, G., 2022. Variation in soil properties and its influence on the dynamic change of soil erosion resistance to overland flow in the water-level fluctuation zone of the Three Gorges Reservoir, China. CATENA 213, 106141. https://doi.org/10.1016/j.catena.2022.106141.

Xiong, M., Leng, G., 2024. Global soil water erosion responses to climate and land use changes. CATENA 241, 108043. https://doi.org/10.1016/j.catena.2024.108043.

Zhang, S., Yang, P., Xia, J., Wang, W., Cai, W., Chen, N., Hu, S., Luo, X., Li, J., Zhan, C., 2022. Land use/land cover prediction and analysis of the middle reaches of the Yangtze River under different scenarios. Sci. Total. Environ. 833, 155238. https://doi.org/10.1016/j.scitotenv.2022.155238.